

Photometric Properties and Scaling Relations of Early Type Brightest Cluster Galaxies

F. S. Liu^{1,2,3*}, X. Y. Xia³, Shude Mao^{4,3}, Hong Wu¹, Z. G. Deng²

¹*National Astronomical Observatories, Chinese Academy of Sciences, A20 Datun Road, Beijing, 100012, P.R.China*

²*Graduate School of the Chinese Academy of Sciences, Beijing, 100049, P.R.China*

³*Department of Physics, Tianjin Normal University, Tianjin, 300074, P.R.China*

⁴*Jodrell Bank Centre for Astrophysics, Alan Turing Building, University of Manchester, Manchester, M13 9PL, UK*

Accepted 23 November 2007, Received 23 November 2007; in original form of 6 August 2007

ABSTRACT

We investigate the photometric properties of the early type Brightest Cluster Galaxies (BCGs) using a carefully selected sample of 85 BCGs from the C4 cluster catalogue with redshift less than 0.1. We perform accurate background subtractions, and surface photometry for these BCGs to 25 mag arcsec⁻² in the Sloan r -band. By quantitatively analysing the gradient of the Petrosian profiles of BCGs, we find that a large fraction of BCGs have extended stellar envelopes in their outskirts; more luminous BCGs tend to have more extended stellar halos that are likely connected with mergers. A comparison sample of elliptical galaxies was chosen with similar apparent magnitude and redshift ranges, for which the same photometric analysis procedure is applied. We find that BCGs have steeper size-luminosity ($R \propto L^\alpha$) and Faber-Jackson ($L \propto \sigma^\beta$) relations than the bulk of early type galaxies. Furthermore, the power-law indices (α and β) in these relations increase as the isophotal limits become deeper. For isophotal limits from 22 to 25 mag arcsec⁻², BCGs are usually larger than the bulk of early type galaxies, and a large fraction ($\sim 49\%$) of BCGs have disky isophotal shapes. The differences in the scaling relations are consistent with a scenario where the dynamical structure and formation route of BCGs may be different from the bulk of early type galaxies, in particular dry (dissipationless) mergers may play a more important role in their formation; we highlight several possible dry merger candidates in our sample.

Key words: galaxies : E/S0s — galaxies: cD — galaxies: cluster of galaxies — galaxies : photometry — galaxies

1 INTRODUCTION

The Brightest Cluster Galaxies (BCGs) are the most luminous and most massive galaxies in the universe. BCGs are located close to the centre of the clusters of galaxies based on the X-ray observations or gravitational lensing observations (e.g., Jones & Forman 1984; Smith et al. 2005). It was noted very early on that some BCGs show an excess of light (‘envelopes’) over the de Vaucouleurs ($r^{1/4}$) profile at large radii (Matthews et al. 1964; Oemler 1973, 1976; Schombert 1986, 1987, 1988; Graham et al. 1996), and a large fraction of BCGs are termed as cD galaxies (e.g., Patel et al. 2006). Although the origin of such extended envelopes is still not completely clear (e.g., Patel et al. 2006), the extended stellar halos of BCGs to surface brightness $\mu(r) < 25$ mag arcsec⁻² are likely from BCGs themselves: the intra-cluster light has much lower surface brightness and only dominates at large

radius ($r \gtrsim 80$ kpc; for detailed discussions, see Zibetti et al. 2005; Bernardi et al. 2007; Lauer et al. 2007).

There has been debate on the formation mechanisms for BCGs and cD galaxies. Several mechanisms have been proposed, such as galactic cannibalism (the merging or capture of cluster satellites due to dynamical friction, Ostriker & Tremaine 1975; White 1976; Ostriker & Hausman 1977), tidal stripping from cluster galaxies (Gallagher & Ostriker 1972; Richstone 1975, 1976; Merritt 1985), and star formation on BCGs by cooling flows (e.g., Fabian 1994). Therefore, it is important to study the photometric properties of BCGs using large and homogeneous BCG samples, which has now become available due to large surveys such as the Sloan Digital Sky Survey (SDSS; for earlier studies, e.g. Postman & Lauer 1995, see references below). Moreover, the statistical properties of the extended envelopes of BCGs may also help to understand how the BCGs form and evolve, especially when combined with high-redshift cluster samples such as EdisCS (White et al. 2005).

* E-mail: lfs@bao.ac.cn

Recently, there has been much progress in this area from both observational and theoretical fronts. Observations show that BCGs have distinct properties from the bulk of elliptical galaxies. The size-luminosity relation and Faber-Jackson relation ($L - \sigma$ relation) for BCGs are significantly steeper than those of non-BCG elliptical galaxies (Lauer et al. 2007; Bernardi et al. 2007; Desroches et al. 2007; von der Linden et al. 2007). It implies that BCGs are larger and have lower velocity dispersions than non-BCG elliptical galaxies, which confirms the pioneering work based on a small BCG sample by Oegerle & Hoessel (1991). The differences between BCGs and non-BCG elliptical galaxies demonstrate that the BCGs may form in a qualitatively different way from non-BCG elliptical galaxies (De Lucia & Blaizot 2007). Furthermore, the steeper $L - \sigma$ relation for BCGs than those of non-BCG elliptical galaxies leads to a contradiction in the prediction of black hole (BH) masses using the $M_{\text{BH}} - \sigma$ or $M_{\text{BH}} - L$ relationships. The usual $M_{\text{BH}} - \sigma$ relation cannot predict black hole masses larger than $3 \times 10^9 M_{\odot}$ in the universe, which is inconsistent with values estimated by other means (Lauer et al. 2007).

Recent simulations and semi-analytic works in the cold dark matter hierarchical structure formation framework provide a plausible picture for the formation of BCGs: they tend to form at high-density peaks when their inhabited dark matter halos collapse at high redshift, and then X-ray driven cooling flows allow a rapid collapse and the formation of a stellar component (Cowie & Binney 1977; Fabian & Nulsen 1977; Fabian 1994). While more than half of the stellar mass in the BCGs may have formed before redshift three, BCGs still grow substantially through dry (dissipationless) mergers when their host massive halos accrete and merge with other halos since redshift one (Gao et al. 2004; De Lucia & Blaizot 2007). This picture is largely consistent with observations, which does not require cooling flows to provide the cold gas if BCGs form late; it also overcomes a potential problem that the merger rate in clusters may be too low due to the high velocity dispersion in dynamically relaxed clusters. Furthermore, dry mergers have been directly observed in cluster environments as well as in the field (e.g., Lauer 1988; van Dokkum 2005; Tran et al. 2005; Bell et al. 2006). However, there are still no systematic investigations on the formation of cD-like BCGs galaxies, especially how the extended stellar halos of cD galaxies form: whether they appear during the dry merger phase, and whether they are the primary cause of the distinct properties of BCGs. There is also no agreement about the contributions of the intra-cluster light (e.g., Gonzalez et al. 2005; Zebetti et al. 2005; Lauer et al. 2007).

The C4 cluster catalogue (Miller et al. 2005) with 748 cluster of galaxies was constructed from the spectroscopic data of Second Data Release (DR2) of the Sloan Digital Sky Survey (SDSS). This is one of the largest published homogeneous database of nearby clusters and groups ($z < 0.17$). In principle, it is suitable for statistical studies of BCGs (see also the more recent, much larger maxBCG catalogue of 13,823 clusters of Koester et al. 2007). Based on BCGs from this published cluster catalogue, or the un-published C4 cluster catalogue selected from SDSS DR3, Bernardi et al. (2007) and von der Linden et al. (2007) find that BCGs have different properties, in particular their scaling laws, from non-BCG early type galaxies. Their results are, how-

ever, not entirely consistent with each other, which could be due to different sample selections or photometry methods. In fact, the slope indices in the size-luminosity and Faber-Jackson ($L - \sigma$) relations found by Bernardi et al. (2007) are also significantly different from those of Lauer et al. (2007), although the trends are the same and these two groups use similar methods to measure luminosities and effective radius R_e ; both are based on fitting the $r^{1/4}$ law to the R -band surface brightness profiles within 50 kpc or to some surface brightness limit of the BCGs. However, the samples they used are different. Lauer et al. (2007) use their own all sky, volume limited ($z < 0.05$) survey of 119 BCGs with precise ground-based surface photometry (Postman & Lauer 1995). Therefore, it is worth investigating whether sample selections and photometry can lead to inconsistencies on scaling laws. In this paper, we construct a different, nearby (with redshift $z < 0.1$) BCG sample based on the C4 cluster catalogue, and perform our own photometry. In particular, we examine how the scaling relations change when different isophotal limits are applied, and compare the results with those of Bernardi et al. (2007), Lauer et al. (2007) and von der Linden et al. (2007).

The outline of the paper is as follows. In §2 and §3 we describe the selection of our local BCG sample and photometric data reduction. We present our main results in §4 and finish with a discussion & summary in §5. Throughout this paper we adopt a cosmology with a matter density parameter $\Omega_m = 0.3$, a cosmological constant $\Omega_\Lambda = 0.7$ and a Hubble constant of $H_0 = 70 \text{ km s}^{-1} \text{ Mpc}^{-1}$ ($h \equiv H_0/100 \text{ km s}^{-1} \text{ Mpc}^{-1} = 0.7$).

2 SAMPLE

Our early type BCG sample is drawn from the early version of the C4 cluster catalogue (Miller et al. 2005). Given that BCGs are located near the centre of clusters of galaxies which is often crowded with galaxies and contaminated by intra-cluster light, to ensure the reliable photometric measurement with high enough S/N ratio for each sample BCG to $\mu(r) < 25 \text{ mag/arcsec}^2$ that is significantly higher than the intra-cluster light (Zibetti et al. 2005; Lauer et al. 2007; Bernardi et al. 2007), we restrict our BCG sample to be brighter than 14.5 mag in the SDSS r -band model magnitude. After we exclude 10 duplicated objects (Bernardi et al. 2007), there are 114 galaxies selected out of a total of 748 BCGs in the C4 cluster catalogue.

Due to fiber collisions in the spectroscopic data, it is necessary to incorporate the SDSS photometric catalogue to avoid missing BCGs using the C4 algorithm. The DR2 version of the C4 catalogue tried to correct for this by selecting the brightest cluster galaxy based on the photometric catalogue. However, as several works (e.g., Bernardi et al. 2007; von der Linden et al. 2007) noticed, some stars or spiral galaxies (some of these are located at the edge of clusters) have been mis-classified as BCGs. We thus performed visual inspections of two-colour images in the g -band and r -band for all the 114 BCG candidates and their clusters in a region of $200 \text{ kpc} \times 200 \text{ kpc}$ and $2 \text{ Mpc} \times 2 \text{ Mpc}$, respectively. We found that C4 1024, C4 2092, C4 2097, C4 2031, C4 2109, C4 3021 and C4 3268 are seriously contaminated by adjacent bright stars or foreground galaxies; C4 3047 is located

at the edge of the corrected frame (Stoughton et al. 2002); C4 3235 is a star; C4 2178 and C4 3257 are nearly edge-on galaxies with dust lanes. In addition, there are 5 objects (C4 1265, C4 1332, C4 2130, C4 3098, and C4 3205) whose parent cluster richness, defined as the number of galaxies within $1 h^{-1}$ Mpc, is less than 10, and hence they may be wrong identifications. In the remaining 98 objects, there are 10 BCGs that are late type galaxies with obvious spiral arms (C4 1023, C4 1053, C4 1324, C4 1366, C4 2001, C4 3016, C4 3143, C4 3246, C4 3282, and C4 3286). These are also excluded from our early type BCG sample, leaving us with 88 possible early-type BCGs. We further excluded 3 objects (C4 1048, C4 1186 and C4 3285) with $M_{r,25} > -21$ that are fainter than L^* galaxies ($M_r^* \sim -21.12$ for $h = 0.7$, see Blanton et al. 2003a) and they are unlikely BCGs (Bernardi et al. 2007). The detailed information for all 29 rejected objects are listed in Table 1. Our final sample consists of 85 BCGs that are in the redshift range of $0.03 \leq z \leq 0.09$ and r -band (model) apparent magnitude in $\sim 13.5 < \text{mag} \leq 14.5$.

Furthermore, we carefully searched for the second ranked cluster galaxies in the 85 C4 clusters and found that the BCGs are about 1.6 mag brighter on average than the second ranked cluster galaxies for the r -band absolute magnitude at $25 \text{ mag arcsec}^{-2}$. Only 6 BCGs have absolute magnitudes within 0.5 mag of the second ranked cluster galaxies. During this process, we found one mis-identified BCG for C4 2020 (Abell 0119), the brightest galaxy in this cluster is UGC 00579, instead of ARK 021 as listed in the C4 catalog. We caution that such cases may also exist in the unpublished C4 catalogue based on the DR3 of the SDSS (see von der Linden et al. 2007).

Notice that there are 4 BCGs (C4 2049, C4 1176, C4 3311 and C4 1035) in our BCG sample described above with obvious merger features. C4 2049, 1176 and 1035 are merger galaxies with two close nuclei and C4 3311 is with clear asymmetrical shapes. We will discuss these four objects in more detail in §4.2.

In order to perform direct comparisons with non-BCGs, we construct a control sample of normal early-type galaxies from the SDSS DR2 spectroscopic catalogue with galaxy velocity dispersion measurement in the MPA `gal_info` catalogue¹. These control galaxies are chosen to be in the same redshift and apparent magnitude ranges as sample BCGs, i.e., $0.03 \leq z \leq 0.09$ and $13.5 \leq \text{mag} \leq 14.5$. 244 early-type galaxies are selected as the control sample after excluding nearly edge-on objects (most of them have dust features), contaminated sources, and objects identified as C4 BCGs. The distributions of the corrected redshifts relative to the Local Group (see Blanton et al. 2005), $(m_{g,25} - m_{r,25})$ colour, and absolute magnitudes at $25 \text{ mag arcsec}^{-2}$ for these two samples are shown in Fig. 1. It can be seen that the control sample has a lower redshift range than those of BCGs. This is because non-BCGs are intrinsically fainter than the BCGs² (see the bottom panel), so for the same magnitude

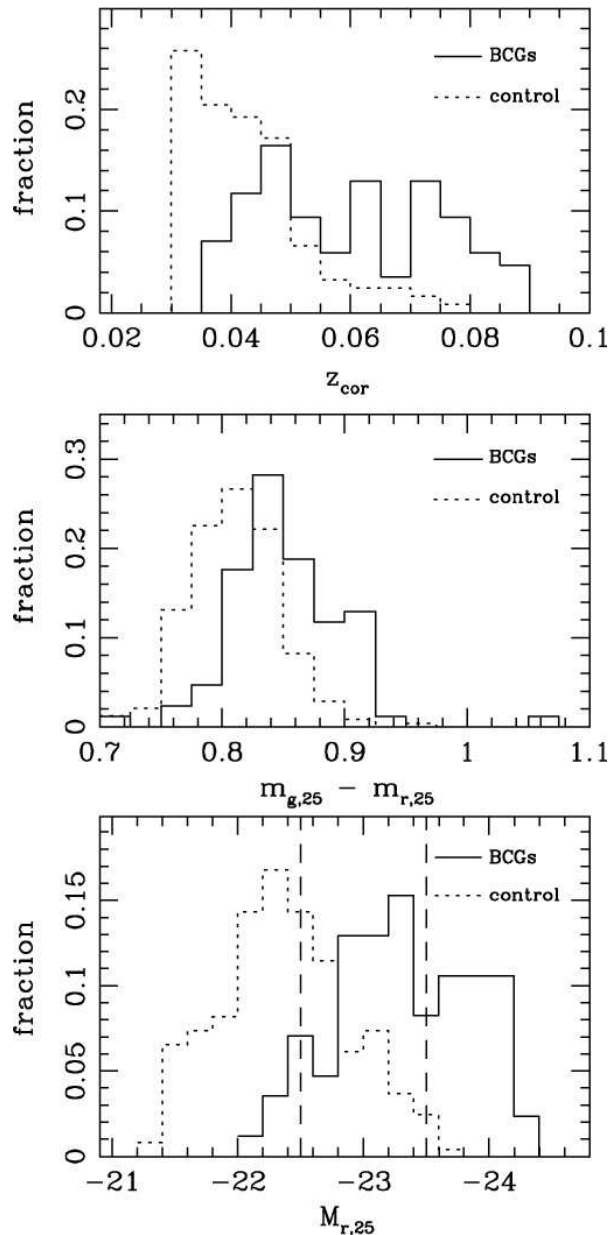


Figure 1. Distributions of corrected redshifts (top panel), $(m_{g,25} - m_{r,25})$ colour (middle panel), and absolute magnitudes at $25 \text{ mag arcsec}^{-2}$ (bottom panel) in the r -band for 85 sample BCGs (solid) and 244 control galaxies (dotted) respectively. Two vertical dashed lines in bottom panel show $-23.5 \leq M_{r,25} \leq -22.5$, where the two samples have a significant overlap. We will compare scaling relations for these two subsamples in §4.4.

limit, they reside more locally. Therefore, it is difficult to construct a control sample in the same luminosity range as that of BCGs. Instead we attempt a comparison in a narrow luminosity range, $-23.5 \leq M_{r,25} \leq -22.5$ (indicated by two vertical dashed lines at the bottom panel of Fig. 1) where there are sufficient overlaps between the control sample and BCGs (see §4.4 for comparisons). Furthermore, both sam-

because we measure the magnitudes to $25 \text{ mag arcsec}^{-2}$, which corresponds to a larger physical size than the radius used by them.

¹ http://www.mpa-garching.mpg.de/SDSS/DR4/raw_data.html

² Bernardi et al. (2007) found that all galaxies brighter than -24 in the r -band are BCGs. Lin & Mohr (2004) found that BCGs are about one magnitude (0.83) brighter on average than the second ranked cluster galaxies even within a small metric radius of $13.7h^{-1}$ kpc. This does not contradict with the larger difference (1.6 mag on average) we found for our BCG sample

ples have colour ($m_{g,25} - m_{r,25}$) ≥ 0.7 , implying that all of them are early type galaxies colour-wise (see Blanton et al. 2003b; Shen et al. 2003 and reference therein). Also the concentration index $C = R_{90}/R_{50}$ for virtually all our galaxies is larger than 2.6, again consistent with their being early-type galaxies (Shimasaku et al. 2001; Strateva et al. 2001). All the basic parameters for these 85 BCGs are listed in Table 2.

3 DATA REDUCTION

3.1 Estimation of the Sky Background

Given that the SDSS image survey in the u - and z -bands are relatively shallow and the i -band images suffer from the ‘red halo’ effect (e.g., Michard 2002; Wu et al. 2005), we use the g - and r -band images in this work. The corrected frames have already been processed by the SDSS photometric pipeline (PHOTO), including bias-subtraction, flat-fielding, cosmic ray removal and corrections for pixel defects. We use the astrometry for these two bands obtained by the SDSS astrometry pipeline (ASTROM), which has a typical error of less than $0.1''$ (Stoughton et al. 2002). On the other hand, for reasons we will discuss below we perform our own photometry.

Although the images from the SDSS archive were processed with photometric corrections, as Wu et al. (2005) pointed out, some spurious features still exist in some images. The spatial variation of these features was about 1-2 ADU. Without corrections, target galaxies that happen to be located within such features will have inaccurate background subtraction and poor surface brightness profiles, especially in the outskirts of the images. We thus first correct for these structures following Wu et al. (2005) before constructing the sky background model below.

As Lauer et al. (2007) pointed out that the SDSS photometric reduction systematically under-estimates the luminosities and half-light radius of BCGs. This arises because the PHOTO pipeline often over-estimates the sky background for galaxies with large size and/or in crowded fields. Both problems are present for BCGs. As a result, Bernardi et al. (2007) performed their own photometric reductions for their sample. On the other hand, von der Linden et al. (2007) address this problem by adding up to 70% of the difference between the local (256×256 pixels) and the global (2048×1498 pixels) sky background (both are available from PHOTO) around the BCGs to the radial surface brightness profiles and the photometry. However, the sky background in the SDSS frames often shows spatial gradients and asymmetry (see the third row of Fig. 2 for an example). Therefore, adding a constant background value to the radial surface brightness profiles may not yield the most accurate photometry, at least on one-to-one basis (see Fig. 4 for comparisons). Therefore, we performed our own photometry following the method of Zheng et al. (1999) and Wu et al. (2002), which was developed to perform deep photometry for nearby large spiral galaxies. This method has been applied to NGC 5907 and NGC 4565, which achieved accurate photometry down to an isophotal limit of ~ 29 mag arcsec $^{-2}$ in the intermediate bands of the BATC system (Fan et al. 1996).

To obtain accurate information of the sky background, we first generate a 2048×1498 pixels ($13.5' \times 9.8'$) background-only image using SExtractor (Bertin & Arnouts 1996) by masking all the detected objects with counts above 1σ noise (of the whole frame) in a frame smoothed by a circular Gaussian with a standard deviation $\sigma = 3$ pixels. As most of sample BCGs have sizes of a few square arcminutes, there are sufficient regions in the masked image to determine the sky background. A median filter with 51×51 pixels is then convolved with the unmasked pixels, after which second-order Legendre polynomials are used to fit both rows and columns respectively (see Zheng et al. 1999 and Wu et al. 2002). The fitted Legendre polynomials are then further smoothed using a circular Gaussian filter with $\sigma = 9$ pixels to obtain our final sky background model. For most BCGs, we find that the sky background is tilted with a spatial variation about 1 – 2 ADU across the whole frame. We can subtract this model from the frame to obtain the sky-free image. Our sky subtraction procedure is similar to that in Gonzalez et al. (2005). Furthermore, the sky background subtracted not only includes the contributions of the intra-cluster light (which is at a much lower level), but also from other astrophysical sources (dust emission etc., see Gonzalez et al. 2005 for a discussion).

Our procedure is illustrated in Fig. 2 for C4 3086. The first, second and third rows of Fig. 2 show the frame, the masked frame and the smoothed sky background in the r -band. Notice that the sky background shows a gradient across the frame. The bottom panels show the distributions of counts in the sky-subtracted frame for all unmasked pixels and for the local vicinity around the target BCG. If the sky background model is successful, then we expect the background counts to follow a Gaussian distribution with a mean close to zero. This is indeed the case, as can be seen from the bottom panels of Fig. 2. The distributions in the r -band for the whole image and the local region are well-fit by Gaussians with dispersion of 5.52 ADU and a mean value of about -2×10^{-2} ADU.

After background subtraction, we geometrically align the two-colour frames, and then trim the corrected frames to 501×501 pixels centred on the target. We run SExtractor again on the trimmed frame to generate a ‘SEGMENTATION’ image, which identifies all objects with flags in the frames. A mask image with all the detected objects except the galaxy of interest flagged can then be obtained from the ‘SEGMENTATION’ image. We carefully examined all the mask images in two colours and corrected a few bad images manually to create good mask images for all galaxies. Photometry is then performed on the trimmed images with the masked areas excluded from the reduction; we discuss the details below.

3.2 Isophotal photometry

To compare the scaling relations, such as the size-luminosity relation and Faber-Jackson relation, of BCGs with those of the bulk of elliptical galaxies, we need to perform accurate surface photometry. In this work, we measure the isophotal magnitudes within a certain radius, instead of magnitudes based on a model (e.g., a de Vaucouleurs [1948] model or a Sérsic [1968] model) as a large fraction of BCGs is not well described by such simple models. Furthermore, to see how

Table 1. Reasons for the rejection of 29 out of 114 C4 BCGs.

C4 ID (1)	R.A.(J2000) (2)	Dec.(J2000) (3)	reason for rejection (4)
1023	153.664827	-0.830910	late type
1053	228.307961	4.287565	late type
1324	223.045968	-0.256108	late type
1366	223.396096	0.010394	late type
2001	350.862674	14.325841	late type
3016	187.452774	64.033013	late type
3143	247.104069	41.168463	late type
3246	136.572283	50.089290	late type
3282	249.318427	44.418227	late type
3286	184.232511	63.409922	late type
1024	226.688031	-1.231709	contaminated by bright star
2031	324.773334	-0.706191	contaminated by bright star
2092	24.225138	-0.533071	contaminated by bright star
2097	338.797166	-1.049529	contaminated by bright star
2109	24.314061	-9.197611	contaminated by bright star
3268	239.339150	54.671105	contaminated by bright star
3021	247.489689	40.630707	contaminated by foreground spiral
2178	351.297310	15.199853	edge-on galaxy with dust lane
3257	249.074493	44.135700	edge-on galaxy with dust lane
3235	119.610850	37.732302	a star
3047	158.245415	56.748148	at the edge of the frame
1265	168.680626	4.024536	richness < 10
1332	167.820450	-0.824176	richness < 10
2130	50.701678	-6.694635	richness < 10
3098	246.907102	42.638233	richness < 10
3205	135.367430	55.044549	richness < 10
1048	147.895859	1.112059	$L < L^*$
1186	183.990581	3.305910	$L < L^*$
3285	259.895020	56.630066	$L < L^*$

the scaling relations vary as a function of isophotal limits, we measure the photometric parameters to four different surface brightness limits, 22, 23, 24, and 25 mag/arcsec². We emphasize that the photometry for the control sample has been performed in the same manner as that for BCGs.

The surface photometry analysis is performed following Wu et al. (2005). We briefly outline the procedures below; the readers are referred to that paper for more details. The ISOPHOTE/ELLIPSE task in IRAF is used to fit each of the trimmed background-subtracted images with a series of elliptical annuli from the centre to the outskirts. The width of annuli is chosen to increase uniformly in logarithmic steps, with the semi-major axis radius increasing by 10% between two adjacent annuli. The size of the annuli in the outer parts is therefore larger, which suppresses the shot noise in the outer regions where the signal-to-noise ratio (S/N) is lower. The ellipticity, position angle, and other quantities are also fitted simultaneously. The r -band images are first used to define the isophotal annuli, which are then applied to the g -band images. The coordinates of the photometric peak in both r -band and g -band are obtained by the DAOPHOT package and are fixed during fitting.

We estimate the seeing of our galaxies in two colours by averaging the star profiles in the corresponding frames respectively. The average values of the FWHMs of the seeings in both colours are $\sim 1.6''$, which are similar to the measurements by the SDSS collaboration. We integrate the observed surface brightness profiles directly to estimate the

isophotal apparent magnitudes and half-light radius R_{50} , within which half of the integrated flux of galaxies is contained, under each isophotal limit. The absolute magnitude (M) is derived from the obtained isophotal apparent magnitude (m) by $M = m - 5 \log(D_L/10 \text{ pc}) - A - k$, taking into account the extinction (A) in each filter by the SDSS, and the k -correction (using the KCORRECT algorithm of Blanton & Roweis 2007). Other photometric parameters, such as ellipticities, coefficients of lowest order deviations from perfect ellipse a_4 and b_4 (see Bender et al. 1988), are derived following Hao et al. (2006). Notice that the a_4/a parameters are weighted by the intensity between twice the seeing radius and the radius where the surface brightness is 25 mag arcsec⁻² in the r -band. We discuss the isophotal shapes in Sect. 4.3.

All our radial profiles in this paper use the equivalent radius of an ellipse, \sqrt{ab} , where a and b are the lengths of semi-major and semi-minor axes of the ellipse. The surface brightness profiles in the two bands are performed accounting for the Galactic extinction correction, cosmological dimming, and the k -correction (Blanton & Roweis 2007). The photometric errors are estimated as in Wu et al. (2005). The observational errors in the surface brightness profiles in each band include random errors (e.g., readout noise, the shot noise of the sky background and BCGs) and the error from the sky subtraction.

To illustrate the performance of our photometry, we show the comparison of our determined Petrosian param-

Table 2. Basic parameters for 85 Brightest Cluster Galaxies.

C4 ID	R.A. (J2000)	Dec. (J2000)	z_{cor}	σ_g (km/s)	D_{lum} (6)	R_{lum} (kpc)	ϵ	a_4/a_1 (10^{-2})	$m_{g,25}$ (10)	$m_{r,25}$ (mag)	$M_{r,25}$ (mag)	$R_{50,25}$ (kpc)	$(\mu_{50,25})_g$ (mag/arcsec $^{-2}$)	$R_{50,25}/R_{50,25,g}$ (15)
2025	7.368340	-0.21260	0.06047	255.51±8.22	0.15	5.06	0.134±0.0022	0.09±0.13	15.11±0.01	14.25±0.01	-22.99±0.02	9.27±0.46	20.41±0.01	3.08±0.19
2006	10.42920	-0.43940	0.05523 ^a	242.90±6.52	0.33	7.29	0.3360±0.0030	-1.77±0.43	14.78±0.01	13.95±0.01	-23.08±0.02	12.64±0.42	20.99±0.01	2.89±0.11
2055	13.87660	-0.93860	0.05644	329.51±6.97	0.51	6.14	0.0940±0.0017	0.22±0.10	14.91±0.01	14.11±0.01	-22.97±0.02	9.00±0.43	20.37±0.01	3.26±0.18
2020	14.06715	-1.25537	0.04503	276.19±5.88	1.01	16.34	0.2672±0.0018	-0.86±0.12	13.15±0.01	12.23±0.01	-23.82±0.02	14.64±0.42	20.58±0.01	3.19±0.10
2033	14.26870	-0.87520	0.04471	329.98±5.76	0.76	7.17	0.1930±0.0013	0.01±0.09	13.44±0.01	13.02±0.01	-24.32±0.02	32.23±0.35	21.78±0.01	2.55±0.03
2030	14.43770	-0.41940	0.07156 ^a	313.40±6.61	0.80	6.82	0.2500±0.0017	-0.11±0.11	13.03±0.01	13.18±0.01	-23.54±0.03	10.17±0.35	20.08±0.02	3.60±0.11
2049	16.84110	14.27320	0.07156 ^a	223.98±4.60	1.09	12.51	0.3300±0.0031	-0.69±0.08	14.51±0.01	13.64±0.01	-24.09±0.02	14.35±0.56	20.26±0.04	3.76±0.12
2004	15.51650	0.43080	0.04765	258.69±5.07	0.35	4.28	0.1354±0.0013	0.34±0.08	14.22±0.01	13.54±0.01	-23.21±0.02	8.64±0.37	20.51±0.01	3.31±0.14
2013	18.74000	13.46330	0.06038	258.69±5.07	0.64	11.97	0.1150±0.0018	0.15±0.13	15.01±0.01	13.36±0.01	-23.06±0.02	10.74±0.35	20.20±0.01	3.73±0.10
2104	20.32340	-0.59760	0.05480	236.39±5.37	0.28	7.98	0.2645±0.0029	0.17±0.11	15.07±0.01	14.18±0.01	-22.76±0.02	8.68±0.46	20.40±0.01	3.41±0.10
2148	24.34640	-0.27050	0.04113	198.57±4.44	0.51	9.24	0.1232±0.0022	0.42±0.20	14.82±0.01	13.98±0.01	-22.37±0.03	4.70±0.42	19.17±0.00	4.14±0.41
2039	28.57530	-0.10580	0.07942	314.91±6.70	1.14	9.27	0.3938±0.0019	0.32±0.10	14.61±0.01	13.17±0.01	-24.08±0.02	24.18±0.50	21.40±0.01	3.02±0.09
2010	30.07060	-1.12780	0.04296	265.27±5.87	1.46	21.78	0.2803±0.0012	-0.63±0.14	14.15±0.01	13.80±0.01	-23.32±0.02	12.78±0.34	20.78±0.01	3.15±0.07
2074	51.52570	-0.61570	0.03762	278.62±5.74	0.37	5.36	0.2316±0.0018	-0.28±0.19	14.15±0.01	13.09±0.01	-23.06±0.03	14.10±0.30	21.25±0.01	3.31±0.05
3129	118.93400	45.87690	0.05123	264.24±6.01	1.32	5.37	0.2982±0.0012	0.53±0.12	14.98±0.01	14.11±0.02	-23.21±0.02	15.82±0.56	20.93±0.01	3.01±0.16
3048	119.18450	45.87690	0.04236	384.95±6.64	0.99	17.04	0.1582±0.0017	-0.10±0.10	14.56±0.01	13.74±0.01	-22.48±0.03	4.65±0.41	20.91±0.01	3.43±0.12
3151	120.70420	39.90600	0.04180 ^a	225.01±3.17	0.54	5.83	0.3174±0.0010	0.99±0.05	14.74±0.01	13.93±0.01	-22.63±0.03	4.65±0.41	20.91±0.01	3.85±0.24
3062	122.59700	42.27300	0.06366	370.33±8.13	0.31	3.66	0.0689±0.0016	0.04±0.04	14.55±0.01	13.70±0.01	-22.56±0.02	5.16±0.39	19.57±0.01	4.88±0.34
1206	131.12790	2.29490	0.05009	225.01±3.17	0.30	9.46	0.1730±0.0007	0.15±0.04	15.10±0.01	13.29±0.01	-23.32±0.02	9.59±0.36	20.14±0.01	3.71±0.13
3110	131.97110	53.87620	0.04505 ^a	370.33±8.13	1.33	17.81	0.1620±0.0018	0.27±0.12	14.85±0.01	13.97±0.01	-23.32±0.02	19.09±0.64	20.86±0.01	2.85±0.16
3105	134.65221	54.31740	0.08618	411.54±5.73	0.29	4.08	0.3072±0.0008	-1.02±0.08	14.46±0.01	13.42±0.01	-22.64±0.02	8.06±0.36	20.08±0.01	3.45±0.16
3102	139.80250	54.85700	0.04572 ^a	291.54±5.53	0.01	8.25	0.2285±0.0015	1.09±0.05	15.30±0.01	14.42±0.01	-23.02±0.02	5.78±0.43	19.74±0.01	3.09±0.26
3263	140.57221	-0.54690	0.05562	235.91±5.41	0.37	7.52	0.2137±0.0018	-0.57±0.04	15.06±0.01	13.34±0.01	-23.29±0.02	10.68±0.36	20.42±0.01	2.93±0.10
3063	151.31219	53.14900	0.04658	259.91±4.88	1.17	6.47	0.0549±0.0010	0.63±0.10	14.52±0.01	13.23±0.01	-22.91±0.02	4.77±0.35	19.66±0.01	4.04±0.26
3055	159.30119	57.05500	0.04556	259.91±4.88	1.17	6.47	0.1174±0.0014	-0.42±0.08	14.52±0.01	13.74±0.01	-22.91±0.02	10.15±0.36	20.69±0.01	3.13±0.11
3055	159.30119	50.12060	0.04573 ^a	285.68±6.68	0.50	8.08	0.2867±0.0020	0.17±0.07	14.06±0.01	13.21±0.01	-23.38±0.02	9.69±0.36	20.54±0.01	3.57±0.13
1076	159.70950	4.64750	0.06815	285.68±6.68	1.44	9.22	0.3052±0.0020	1.07±0.15	14.66±0.01	13.41±0.02	-23.79±0.02	20.04±0.52	21.36±0.01	2.59±0.09
3232	162.30040	0.07988	0.07988	273.08±7.90	0.64	10.00	0.2076±0.0011	0.35±0.08	15.07±0.01	14.19±0.01	-23.49±0.02	12.69±0.55	20.59±0.01	2.88±0.18
3094	162.42300	56.64130	0.04653	279.86±6.40	0.65	15.28	0.2680±0.0008	0.61±0.05	14.82±0.01	13.98±0.01	-22.65±0.02	5.61±0.36	19.66±0.01	3.82±0.23
1156	162.49519	0.32230	0.03836	290.36±5.20	0.66	4.04	0.2916±0.0011	0.46±0.08	14.09±0.01	13.30±0.01	-22.88±0.03	7.22±0.30	19.98±0.01	3.74±0.12
3032	162.89661	55.46880	0.04095	214.53±6.62	1.15	5.92	0.1943±0.0025	-1.58±0.15	14.92±0.01	14.13±0.01	-22.53±0.03	5.54±0.36	19.76±0.01	3.04±0.10
3081	163.34550	56.31450	0.07305 ^b	...	0.80	15.69	0.2844±0.0018	0.09±0.15	15.11±0.01	14.25±0.01	-23.46±0.02	13.97±0.56	20.82±0.01	3.00±0.18
1110	164.50481	1.60460	0.03970 ^a	...	1.07	11.02	0.1607±0.0014	-0.13±0.09	13.92±0.01	13.10±0.01	-23.16±0.03	13.25±0.31	21.02±0.01	3.21±0.06
3311	166.06110	57.40260	0.04734	256.25±5.30	1.04	10.42	0.2361±0.0014	-1.20±0.09	14.23±0.01	13.50±0.01	-23.17±0.03	4.72±0.37	18.77±0.00	4.06±0.30
3012	168.06959	57.07600	0.04732	305.47±6.53	0.14	9.80	0.1882±0.0012	0.12±0.07	14.53±0.01	13.70±0.01	-22.97±0.02	0.81±0.37	19.70±0.00	3.56±0.19
1035	172.87219	-1.66800	0.04554	...	0.55	8.36	0.1357±0.0009	-1.32±0.08	14.46±0.01	13.63±0.01	-22.80±0.02	1.98±0.34	13.20±0.23	3.72±0.23
1031	172.87219	5.10150	0.07544	280.02±8.41	0.78	9.12	0.1325±0.0022	-0.07±0.13	14.46±0.01	14.15±0.01	-23.68±0.02	12.30±0.57	20.43±0.01	3.24±0.22
1038	179.37070	0.07858 ^a	0.92	6.63	0.2500±0.0018	0.32±0.10	15.07±0.01	14.18±0.01	-23.68±0.02	11.88±0.59	20.26±0.01	3.48±0.27
3035	180.77960	51.07320	0.06552	...	0.64	7.85	0.2260±0.0014	-0.12±0.09	15.01±0.01	14.14±0.01	-23.21±0.02	21.18±0.48	20.60±0.01	3.11±0.17
1015	182.57010	5.38600	0.07965	263.95±9.32	2.74	12.04	0.1891±0.0021	-0.40±0.14	14.60±0.01	13.76±0.01	-24.01±0.02	14.96±0.57	21.58±0.02	2.36±0.08
1142	183.66470	5.46780	0.07730	224.57±7.94	0.28	6.20	0.1983±0.0014	-0.02±0.11	15.17±0.01	13.92±0.01	-23.51±0.02	13.38±0.58	20.69±0.01	3.28±0.22
3019	183.70261	59.90620	0.06040 ^b	261.49±6.90	1.33	8.64	0.2179±0.0015	-0.42±0.09	14.71±0.01	13.51±0.01	-23.35±0.02	12.90±0.46	20.77±0.01	2.81±0.12
1058	184.71820	5.24570	0.07659 ^b	...	1.05	10.35	0.1821±0.0025	-0.19±0.16	14.68±0.01	13.84±0.01	-23.97±0.02	19.08±0.57	21.00±0.01	2.94±0.14

ters with those of SDSS in Fig. 3. One can see that the SDSS pipeline under-estimates the sizes (and thus luminosity) of BCGs, which has been pointed out by other workers (e.g., Lauer et al. 2007). There is a systematic trend: the under-estimation becomes more serious for larger (brighter) BCGs. This is in good agreement with the results of Desroches et al. (2007, see their Fig. 1.).

As mentioned before, von der Linden et al. (2007)

adopted a simple prescription to correct for the sky subtraction problem. In Fig. 4 we show a comparison between their surface brightness profile, ours and that from the SDSS for three example galaxies. It can be seen that our results are in very good agreement with those of von der Linden et al. (2007). While there are small differences at faint surface brightness (25 mag arcsec $^{-2}$), such differences have little impact on their results since they adopted a surface brightness

Table 2—Continued

C4 ID	R.A. (J2000)	Dec. (J2000)	z_{cor}	σ_g (km/s)	D_{min} (kpc)	R_{min} (kpc)	ϵ	a_1/a_2 (10^{-2})	$m_r, 25$ (mag)	$m_r, 25$ (mag)	$M_r, 25$ (mag)	$R_{50, 25}$ (kpc)	$(a_{50, 25})^2$ (mag/arcsec 2)	$R_{90, 25}/R_{50, 25}$
(1)	(2)	(3)	(4)	(5)	(6)	(7)	(8)	(9)	(10)	(11)	(12)	(13)	(14)	(15)
3061	186.17821	61.47070	0.07042	274.82±7.19	0.99	18.35	0.1947±0.0022	-0.07±0.16	14.93±0.01	14.06±0.02	-23.54±0.02	13.01±0.53	20.60±0.01	3.19±0.18
1176	189.70480	6.15840	0.07480	...	1.34	7.56	0.2500±0.0023	1.09±0.17	15.10±0.01	14.24±0.01	23.53±0.02	16.44±0.56	21.13±0.03	2.66±0.14
1125	190.55270	-2.14740	0.08280	...	1.14	29.33	0.3059±0.0021	-1.16±0.24	14.95±0.01	14.04±0.02	-23.39±0.02	21.28±0.62	21.25±0.01	2.83±0.14
1065	191.30360	1.80480	0.04703	232.61±6.35	0.54	11.02	0.2300±0.0015	0.19±0.10	14.38±0.01	13.93±0.03	-23.09±0.03	13.03±0.37	21.05±0.01	2.72±0.07
1102	191.71339	0.29700	0.08861	317.09±6.32	0.80	19.61	0.4621±0.0014	-0.86±0.14	15.09±0.01	14.10±0.01	-24.06±0.02	17.64±0.66	20.74±0.01	3.08±0.20
1041	194.67290	-1.76150	0.08393	...	1.04	11.13	0.5222±0.0014	-1.02±0.20	14.75±0.01	13.86±0.01	-24.15±0.02	27.41±0.62	21.60±0.01	2.47±0.10
1052	195.71910	-2.51640	0.08576	...	1.32	15.03	0.2646±0.0051	-0.95±0.36	14.77±0.01	13.86±0.01	-24.12±0.01	23.43±0.64	21.20±0.01	2.82±0.13
3117	199.54410	66.42790	0.06706	311.21±7.14	0.63	4.14	0.2835±0.0018	0.20±0.13	15.03±0.01	14.16±0.01	-23.33±0.02	9.29±0.51	20.08±0.01	3.85±0.28
1022	199.81970	-0.99540	0.08337	...	0.45	17.25	0.2534±0.0022	-0.68±0.18	15.06±0.01	14.16±0.01	-23.84±0.02	17.47±0.62	20.94±0.01	3.13±0.18
1153	201.57359	0.22150	0.08220	...	1.01	6.56	0.2694±0.0018	0.47±0.14	14.78±0.01	13.94±0.01	-24.05±0.02	19.76±0.61	20.99±0.01	2.80±0.14
3011	204.05470	59.20640	0.07144	...	1.56	9.72	0.2328±0.0019	0.26±0.12	14.55±0.01	13.66±0.02	-23.98±0.02	19.55±0.54	21.04±0.02	3.45±0.23
1046	206.10750	2.10990	0.07165	380.69±7.56	1.03	8.71	0.1641±0.0010	-0.51±0.05	14.52±0.01	13.67±0.01	-23.97±0.02	11.30±0.54	19.86±0.01	3.45±0.23
1001	208.27670	5.14970	0.07847	339.72±8.72	1.22	7.10	0.2364±0.0018	-0.86±0.13	14.78±0.01	13.82±0.02	-23.97±0.02	15.54±0.59	20.55±0.01	3.21±0.19
1187	211.91200	-0.95530	0.05343	276.48±5.86	0.20	8.30	0.2365±0.0011	0.21±0.08	14.68±0.01	13.88±0.01	-23.14±0.02	9.99±0.41	20.43±0.01	3.64±0.16
1162	216.19749	2.66440	0.05536	254.69±5.18	0.77	6.08	0.1556±0.0018	-0.51±0.10	14.87±0.01	14.03±0.01	-22.90±0.02	8.71±0.41	20.37±0.01	3.06±0.16
1133	217.41930	0.36640	0.05531	304.26±4.46	1.48	10.20	0.0715±0.0012	0.18±0.06	15.02±0.01	14.16±0.01	-22.88±0.02	5.69±0.43	19.46±0.00	4.07±0.34
3086	219.09790	60.47130	0.05010	207.45±4.46	0.50	5.73	0.2257±0.0011	0.42±0.07	15.05±0.01	14.23±0.01	-22.57±0.02	6.38±0.39	20.02±0.01	3.43±0.21
1344	226.53990	3.67510	0.03581	255.36±4.64	0.44	4.08	0.2562±0.0011	0.06±0.08	14.54±0.01	13.73±0.01	-22.29±0.03	4.02±0.28	19.29±0.00	4.19±0.22
1065	226.54871	3.14260	0.04222	277.94±6.09	1.20	7.59	0.1716±0.0012	0.64±0.07	14.36±0.01	13.54±0.01	-22.87±0.03	9.60±0.33	20.61±0.01	2.99±0.09
1362	228.09130	4.51750	0.03838	...	0.53	4.26	0.0570±0.0012	-0.18±0.06	14.50±0.01	13.74±0.01	-22.46±0.03	6.05±0.30	20.02±0.01	2.71±0.11
1211	228.09190	3.39680	0.04494	...	1.08	6.15	0.2606±0.0023	-0.48±0.15	14.80±0.01	14.00±0.01	-22.58±0.03	8.94±0.35	20.78±0.01	3.04±0.11
1211	228.25240	2.02610	0.03790	175.07±5.67	0.62	3.25	0.0619±0.0020	-0.09±0.10	14.85±0.01	14.07±0.01	-22.10±0.03	6.55±0.30	20.55±0.01	3.09±0.11
3020	232.31101	52.86390	0.07340	285.68±7.45	0.53	17.03	0.3802±0.0014	-0.38±0.14	14.83±0.01	13.95±0.02	-23.75±0.02	15.81±0.55	20.81±0.01	3.26±0.17
3077	240.36700	53.94740	0.06600	330.21±6.49	1.71	10.78	0.1894±0.0021	-0.21±0.14	14.61±0.01	13.70±0.01	-23.75±0.02	17.85±0.50	21.07±0.01	2.94±0.11
3024	242.40390	53.04130	0.06406	279.19±7.14	0.47	4.02	0.2402±0.0011	-0.73±0.07	15.05±0.01	14.22±0.01	-23.16±0.02	9.24±0.49	20.23±0.01	3.13±0.21
3095	242.76700	52.45030	0.06351	...	0.50	14.14	0.2756±0.0010	-0.99±0.07	14.61±0.01	13.76±0.01	-23.60±0.02	13.79±0.48	20.66±0.01	2.84±0.13
3248	253.57260	37.62240	0.06257	...	1.13	9.78	0.1603±0.0018	-0.93±0.11	15.01±0.01	14.19±0.01	-23.13±0.02	8.80±0.48	20.16±0.01	3.62±0.25
3034	254.08791	39.27520	0.06258	280.66±6.13	1.01	6.66	0.2096±0.0012	0.48±0.09	14.95±0.01	14.08±0.01	-23.24±0.02	11.74±0.48	20.68±0.01	3.12±0.16
3001	255.63811	33.51670	0.08686	333.52±7.51	0.83	11.11	0.1113±0.0015	-0.04±0.09	15.03±0.01	14.10±0.01	-24.00±0.02	14.04±0.64	20.30±0.01	3.41±0.27
3002	258.12900	64.06080	0.07420	285.68±9.49	0.82	9.16	0.1660±0.0020	-0.45±0.12	14.86±0.01	13.95±0.01	-23.78±0.02	18.81±0.56	21.16±0.01	2.59±0.12
2012	328.52530	-8.64290	0.07308	...	1.63	14.99	0.1866±0.0013	0.71±0.09	14.53±0.01	13.70±0.01	-23.99±0.02	20.35±0.55	21.12±0.04	2.54±0.10
2003	329.25720	-7.83960	0.06254	240.66±5.59	0.36	11.07	0.2941±0.0012	0.67±0.07	14.91±0.01	14.05±0.01	-23.22±0.02	9.23±0.48	20.17±0.01	3.34±0.22
2026	331.82071	-7.54380	0.06053	...	0.90	13.51	0.1190±0.0014	0.04±0.08	14.91±0.01	14.05±0.01	-23.21±0.02	8.03±0.46	19.88±0.01	3.67±0.26
2019	334.06500	-9.33330	0.08347	...	0.81	8.15	0.2547±0.0016	-0.51±0.10	14.93±0.01	14.04±0.01	-23.99±0.02	19.91±0.62	21.07±0.01	2.72±0.14
2058	340.02179	-0.80770	0.05386	264.89±6.41	0.45	9.33	0.2698±0.0010	0.43±0.06	15.05±0.01	14.17±0.01	-22.82±0.02	4.56±0.41	19.05±0.01	4.31±0.42
2002	358.55701	-10.41900	0.07810	322.54±7.63	1.39	15.73	0.0554±0.0017	0.30±0.09	14.56±0.01	13.67±0.01	-24.18±0.02	20.07±0.59	20.90±0.01	2.85±0.13

Note. — Col.(1). SDSS-C4 ID for the C4 Clusters. Col.(2). R.A. (J2000). Col.(3). Dec. (J2000). Col.(4). Corrected redshifts relative to the Local Group for BCGs. The values marked with 'a' are from the NASA/IPAC Extragalactic Database (NED) and are corrected following Blanton et al. (2005). Col.(5). Galaxy velocity dispersions within the $3''$ fiber apertures in the MPA *gal-fits* catalogue. Col.(6). Observed D_{min} values in the r -band $d\theta(r)/d\log(r)$ profiles. Col.(7). Radii, R_{min} , for the minimum position of the valley in the r -band $d\theta(r)/d\log(r)$ profiles. Col.(8). Mean ellipticity. Col.(9). Extinction-corrected g -band isophotal apparent magnitudes. Col.(10). Extinction-corrected r -band isophotal apparent magnitudes. Col.(11). Extinction-corrected r -band isophotal apparent magnitudes. Col.(12). r -band isophotal absolute magnitudes. Col.(13). Mean effective half-light radius. Col.(14). Mean effective surface brightness. Col.(15). Concentration factor, $C' = R_{90, 25}/R_{50, 25}$. The quantities in Columns (10-15) are for an isophotal limit of 25 mag arcsec $^{-2}$ in the r -band.

of 23 mag arcsec $^{-2}$ to measure the physical quantities. So for statistical purposes, their method can offer an efficient way of performing photometry, particularly at high surface brightness limits.

4 RESULTS

4.1 The Extended Envelopes of BCGs

As discussed in the introduction, the surface brightness profiles of the majority of cD galaxies show strong deviation from a perfect de Vaucouleurs or Sérsic profile due to cD galaxies embedded in an extensive luminous stellar halo. In order to quantitatively measure the extended envelope of

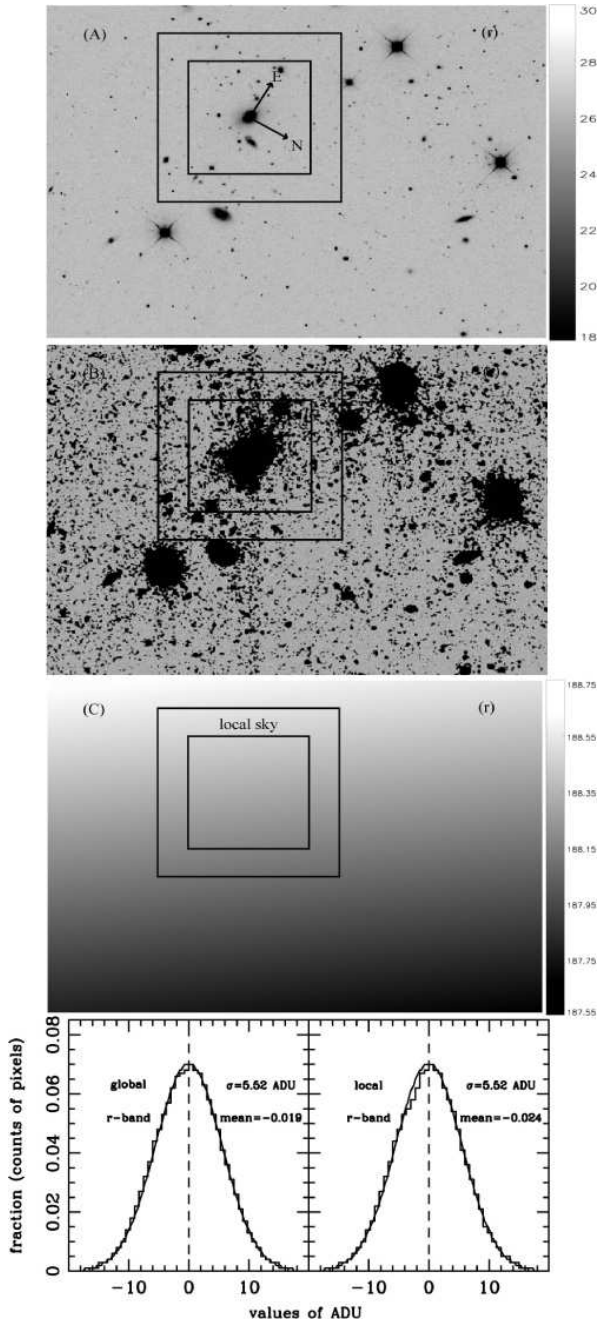


Figure 2. An example of sky subtraction (for target BCG C4 3086) in the r -band. The first row shows the SDSS corrected frame (2048×1498 pixels; $13.5' \times 9.8'$), the second row shows the masked frame, and the third row shows the fitted sky frame. The inner box in each frame has 501×501 pixels ($3.3' \times 3.3'$), and the outer box has 751×751 pixels ($4.7' \times 4.7'$). The bottom panels show the normalised distributions of flux in the unmasked region after the sky background subtraction, for the whole frame (left) and the local region between the two boxes (right) in the r -band. The solid lines in the two panels are the best-fit Gaussians to the distributions.

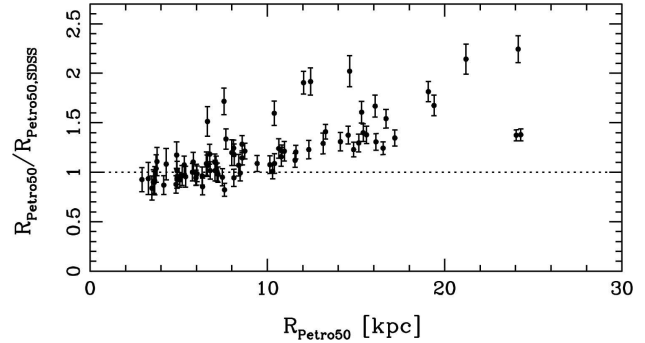


Figure 3. Comparison between our measured Petrosian half-light radii to those provided by the SDSS for our BCG sample.

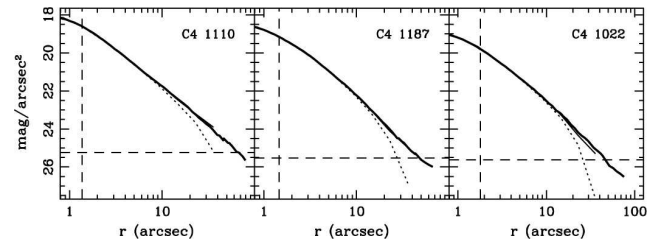


Figure 4. Comparison between the surface brightness profiles obtained using our method (thick solid lines) and those from the SDSS (dotted lines) and von der Linden et al. (2007, thin solid lines) for three example galaxies in the r -band. The vertical and horizontal dashed lines indicate twice seeing radius and one percent of the sky brightness respectively. Notice for the left and middle galaxies, our results almost overlap with those from von der Linden et al. (2007).

BCGs, we use an objective method based on the Petrosian $\eta(r)$ profiles (Patel et al. 2006), defined as

$$\eta(r) \equiv \mu(r) - \langle \mu(r) \rangle, \quad (1)$$

where $\mu(r)$ is the surface brightness in magnitudes at radius r and $\langle \mu(r) \rangle$ is the mean surface brightness within r (Petrosian 1976). There is a distinct signature of a plateau in the Petrosian $\eta(r)$ profiles for cD galaxies with an extended stellar halo (see below). Such a plateau is not present for normal elliptical galaxies which are usually well-fit by a de Vaucouleurs' surface brightness profile (e.g., Kjærgaard et al. 1993; Brough et al. 2005). Furthermore, notice that the plateau is not present for the Sérsic surface brightness profile that better fits some ellipticals (see Fig. 1a of Graham et al. 1996).

Fig. 5 shows the surface brightness profiles and Petrosian $\eta(r)$ profiles for 3 BCGs. For BCG C4 1187, its profile is well fit by a Sérsic with $n \approx 4.53$ (in the g -band) model, and the $\eta(r)$ profile does not show any distinct feature. In contrast, for C4 3034 and C4 3077, their surface brightness profiles deviate significantly from a single Sérsic profile (or the $r^{1/n}$ profile, $n = 4$ for the de Vaucouleur profile), and the $\eta(r)$ profile shows a plateau. Furthermore, we can see that the more significant the deviation of the surface brightness profile from the a single Sérsic profile (i.e., the more prominent the stellar halo in the outskirts), the flatter the plateau in the $\eta(r)$ profile becomes.

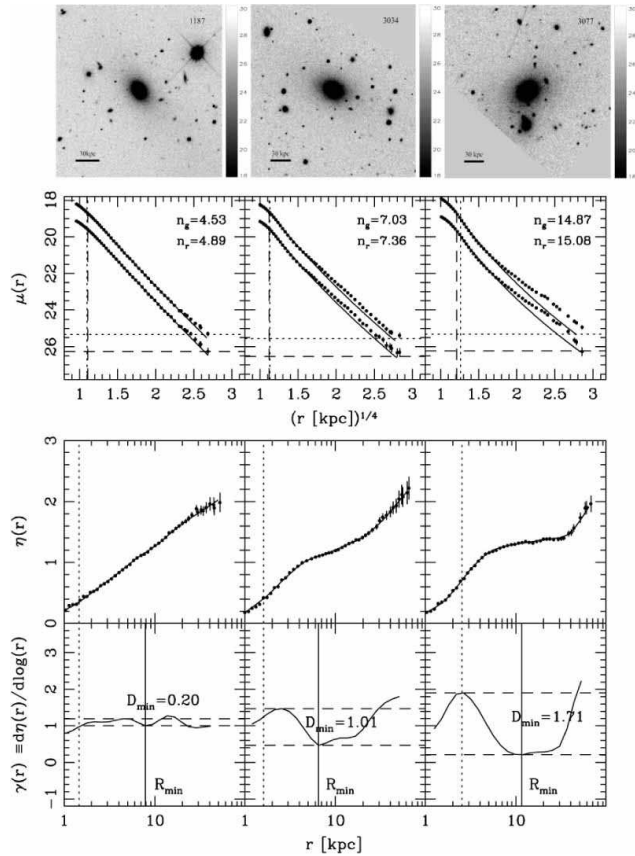


Figure 5. Images, surface brightness, $\eta(r)$ and $d\eta(r)/d\log(r)$ profiles for three typical examples BCGs (C4 1187, C4 3034 and C4 3077). The images shown in the top panels are in the r -band and have a size of 501×501 pixels. In each image, north is up and east is to the left. The second row shows the radial surface brightness profiles in the g -band (lower curve) and r -band (upper curve) respectively. The solid line is the best-fit Sérsic model for each surface brightness profile that is obtained by fitting intensity profile from twice seeing radius to radius at $25 \text{ mag arcsec}^{-2}$ respectively. The vertical and horizontal lines are twice the seeing radius and one percent of the sky brightness in the g -band (dashed lines) and r -band (dotted lines) respectively. The third row shows the observed (dots) and smoothed (line) Petrosian $\eta(r)$ profiles in the r -band. The bottom row shows the corresponding $d\eta(r)/d\log(r)$ profile. The vertical solid line in each panel indicates the minimum position,

To quantitatively determine how a surface brightness profile deviates from the $r^{1/n}$ profile we calculate the gradient of $\eta(r)$, $\gamma(r) \equiv d\eta(r)/d\log(r)$. As mentioned before, a single $r^{1/n}$ model profile always results in a monotonic $\gamma(r)$ profile for any n . The bottom panels of Fig. 5 show this quantity as a function of radius. It is clear that galaxies with the most significant deviation from the model profile also have deeper valleys in the $\gamma(r)$ profile. We label the radius of the minimum in $\gamma(r)$ as R_{min} , and also define a depth, D_{min} , as the difference between the minimum and maximum of $\gamma(r)$ outside twice the seeing radius and R_{min} .

The right histogram in Fig. 6 shows the distribution of D_{min} for our sample BCGs (the median value is ~ 0.8). We can see that the distribution of D_{min} shows a weak bimodality, but is still consistent with a continuous distribu-

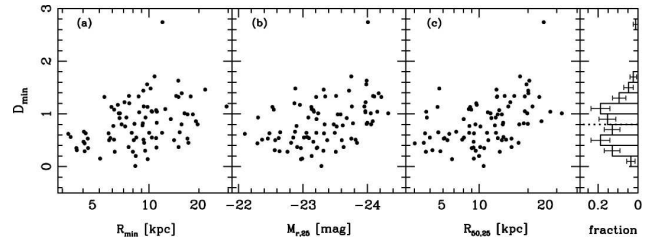


Figure 6. Correlation of D_{min} with R_{min} , r -band absolute magnitude, and size for 85 BCGs, measured out to an isophotal limit $25 \text{ mag arcsec}^{-2}$. The right-most panel shows the histogram of the D_{min} distribution together with the Poisson errors; the median value is ~ 0.8 (indicated by a thick dotted line).

tion within Poisson error bars. This shows that the deviation of the surface brightness profiles from the a single Sérsic profile does not have any sharp transitions. Therefore, it is difficult to give an unambiguous criterion to separate cD galaxies from non-cD BCGs.

The left panel of Fig. 6 shows the correlations between D_{min} and R_{min} . The null-hypothesis that there is no correlation between D_{min} vs. R_{min} can be rejected at the 7.5×10^{-4} level. So statistically the larger the radius R_{min} , the more significant the extended envelope a BCG appears to have. The middle and right panels in Fig. 6 show the correlations between D_{min} with the r -band luminosity and the half-light radius for BCGs. The null-hypothesis that there are no correlations between D_{min} vs. $M_{r,25}$ and D_{min} vs. $R_{50,25}$ can be rejected at the 3.8×10^{-5} , and 9.6×10^{-6} confidence levels. These correlations demonstrate that more luminous and larger BCGs tend to have more extended stellar envelopes and therefore the fraction of cD galaxies increases.

4.2 Mergers and Envelopes in BCGs

As mentioned in §2 that there are four galaxies in our BCG sample that have either two close nuclei or other clear merging signatures, such as broad faint fans or asymmetry in the morphology. The top panel of Fig. 7 shows the image of C4 1176, from which one can clearly see two nuclei and a broad surrounding fan to the north of the image. The SDSS provides the spectra for both nuclei, which are shown in the bottom panels of Fig. 7. From the spectra the redshifts of the two nuclei are 0.0738 and 0.0736 respectively, corresponding to only 60 km s^{-1} difference in the line-of-sight velocity. The angular distance between the two nuclei, $\sim 4.7''$, implies a projected separation of just $\sim 6.7 \text{ kpc}$. Therefore, C4 1176 is most likely a merger galaxy with two nuclei. Furthermore, the spectroscopic properties of these two nuclei are similar; both are typical of early type galaxies with weak emission lines of LINER characteristics, indicating that BCG C4 1176 may be a dissipationless (dry) merger system.

For the other three BCGs, we can see from the top panel of Fig. 8 that C4 2049 and C4 1035 also have two possible close nuclei. From the SDSS spectra, we find that the projected distance between the two nuclei for C4 1035 is only $\sim 1.7 \text{ kpc}$ and the relative line-of-sight velocity is 120 km s^{-1} , and thus may be another merging BCG. For C4 2049, the SDSS has only spectrum for one nucleus. The angular distance between these two nuclei is $\sim 5.5''$. If they are at the same redshift, then the projected distance is

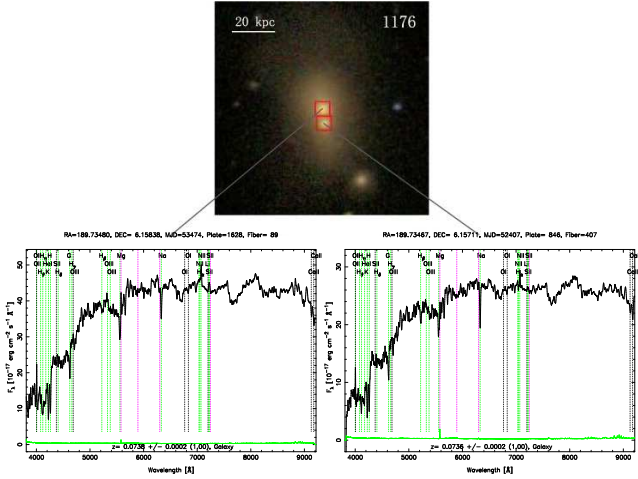


Figure 7. The image of merging BCG C4 1176 with two nuclei shown in the top panel. North is up and east is to the left. The bottom two panels show the spectra of the two nuclei (the line symbols are from SDSS, see http://www.sdss.org/gallery/gal_spectra.html); the redshifts of the two nuclei are almost the same, indicating they are merging. Notice the broad low-surface brightness fan to the north of the image.

~ 7.7 kpc. Hence C4 2049 is another possible merger BCG. For C4 3311, although one cannot see double nuclei at its centre (down to the SDSS spatial resolution), it shows clear asymmetry in shape, which is indicative of merging activities.

The second, third and bottom rows of Fig. 8 show the surface brightness profiles, $\eta(r)$ profiles and $d\eta(r)/d\log(r)$ profiles for all four merger/possible merger BCGs. As can be seen, there are obvious plateaus in the $\eta(r)$ profiles for 3 out of 4 merger BCGs (C4 2049, 1176, and 3311). The D_{\min} values measured from the $d\eta(r)/d\log(r)$ profile are 1.34, 1.34, and 1.04, for C4 2049, 1176, and 3311 respectively, which are much larger than the median D_{\min} value (~ 0.8) for the whole BCG sample. Therefore, these three BCGs clearly have extended envelopes in their outskirts and are likely cD galaxies.

The high fraction of cD galaxies in merger BCGs and the fans corresponding to cD galaxy envelopes suggest that the extended stellar halos of BCGs are from mergers and they appear shortly after merging takes place.

In fact, the role of dry (dissipationless) mergers in the formation of ellipticals has recently received much attention. As pointed out by Bell et al. (2006) and van Dokkum (2005), the typical morphological signatures of dry mergers are broad stellar fans, short tidal tail with similar colour as the galaxy itself, and asymmetries at very faint surface brightness levels. The four examples of merger BCG candidates in our sample shown at Fig. 8 indeed have all these signatures, but they also show even more direct merger signs: in three of these four cases, there are two close nuclei. Fig. 9 shows ten more examples of possible merger systems from our sample. They have broad low-surface brightness fans or distinct asymmetries (top panels); many visually appear to inhabit in environment with multiple small satellites (bottom panels). These images provide strong evidence for the connection of mergers with the formation of stellar halos

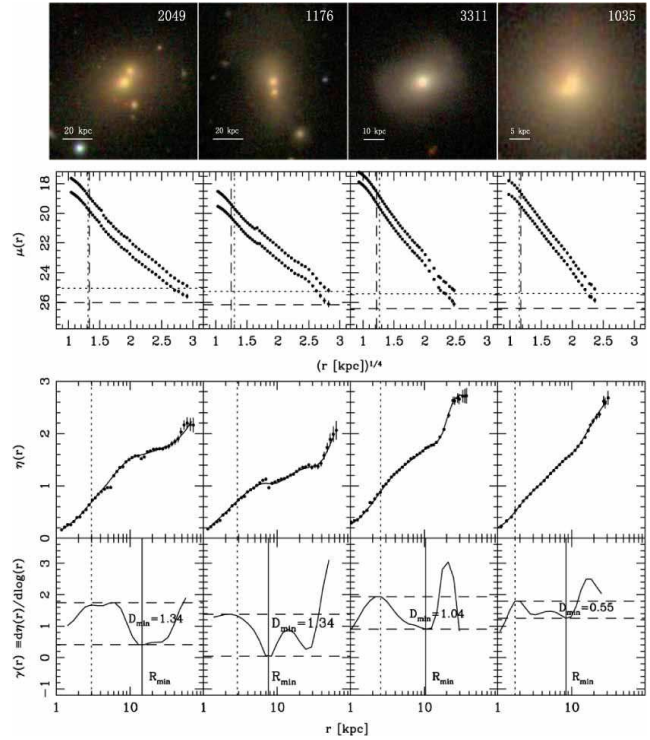


Figure 8. Images, surface brightness, $\eta(r)$ and $d\eta(r)/d\log(r)$ profiles in the r -band for four likely merger BCGs in our sample. The format is the same as in Fig. 5. In each image, north is up and east is to the left.

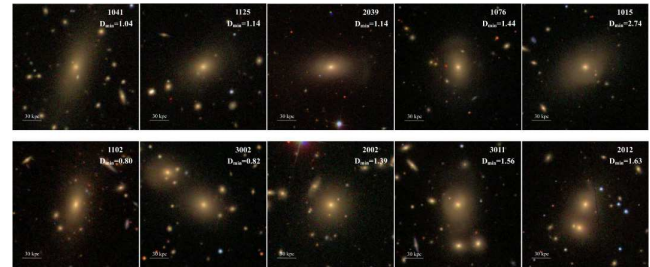


Figure 9. The panels in the top row show the images of BCGs with obvious dry merger signatures, such as broad fans or faint asymmetry shapes. In the bottom row, all 5 images of BCGs are surrounded by many possible satellites or are in pair or triple systems; these are possible signatures of interaction and mergers. The values of D_{\min} for all these dry merger candidates are larger than the median value (0.8) in the D_{\min} distribution for sample BCGs. In each image, north is up and east is to the left.

in BCGs. The 59 BCGs with spectroscopy from SDSS have spectra similar to the examples shown in Fig. 7, indicating our BCG samples are typical early-type galaxies. Their spectra do not show significant star formation at the centre, although one third of our BCGs show weak emission lines with LINER characteristics. Therefore, the mergers appear to be largely dissipationless (dry). We will return to the role of mergers in the formation of BCGs in a future study.

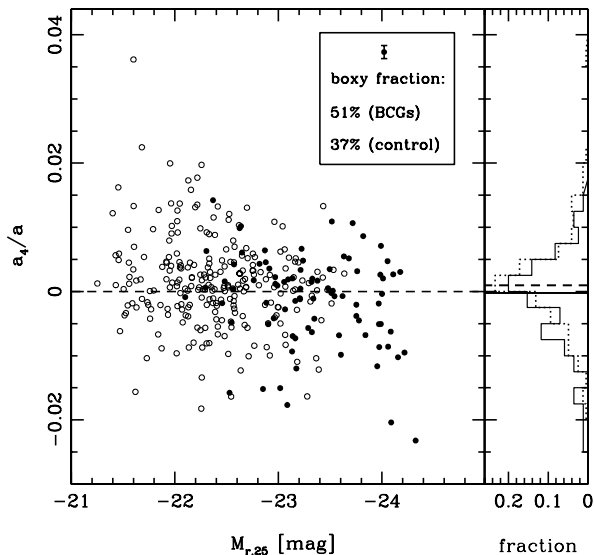


Figure 10. Structure parameter a_4/a versus r -band absolute isophotal magnitude, $M_{r,25}$, for the BCGs (solid circles) and the control sample (open circles) respectively (left panel). The median error bar in a_4/a , and the fractions of galaxies with boxy isophotes for BCGs and the control sample are shown in the inset. The right panel shows the histograms of the a_4/a distributions for the BCGs (solid histogram) and the control sample (dotted histogram). The median values are shown as solid and dashed lines respectively.

4.3 Isophotal Shapes

We also investigated the shapes of isophotes for BCGs and compared with those of the control sample. The isophotes of ellipticals are usually well fit by ellipses. However, small but significant deviations exist, which are usually described by the Fourier components of the deviations. The most significant one is the a_4/a (Lauer et al. 1985; Bender et al. 1989), with a positive (negative) a_4/a indicating a disk (boxy) isophotal shape.

Fig. 10 shows how the a_4/a parameter varies with the luminosity of galaxies for both the BCGs and the control sample. It is clear from Fig. 10 that a_4/a decreases as the luminosity of galaxies increases, hence the fraction of boxy galaxies increases for both samples; this trend has been pointed out by many authors (e.g., Bender et al. 1989; Hao et al. 2006). However, the boxy fraction for BCGs (51%) is not much larger than that of the bulk of ellipticals (37%), even though BCGs are more luminous than the bulk of ellipticals in the control sample. In particular, we can see from Table 2 and Fig. 10 that the boxy fractions of BCGs with luminosities in the range of $-24 \lesssim \text{mag} \leq -23$ and $\text{mag} < -24$ are $\sim 55\%$ and $\sim 65\%$ respectively. So there are still a large fraction of very luminous early type galaxies with disk isophotes ($a_4/a > 0$), which is consistent with the HST image results on BCGs by Laine et al. (2003). Faber et al. (1997) and Lauer et al. (2005) pointed out that galaxies brighter than $M_V = -22$ mag (corresponding to $M_r \approx -22.6$ mag, after correcting the difference in

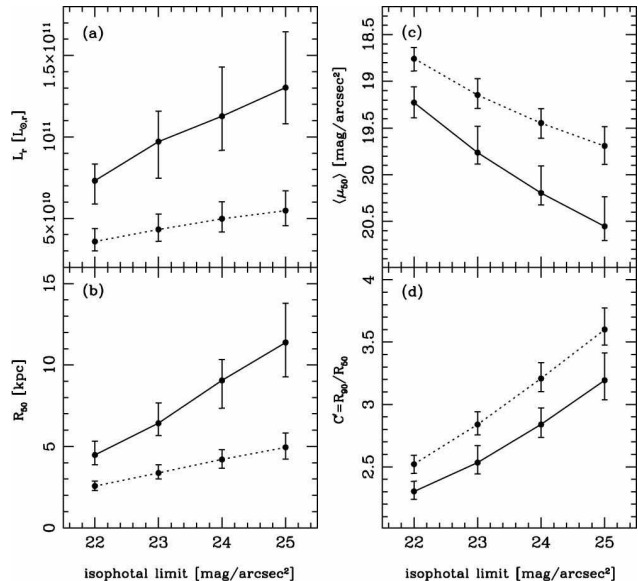


Figure 11. Luminosity (L_r), size (R_{50}), mean surface brightness within R_{50} ($\langle \mu_{50} \rangle$) and the concentration factor ($C' = R_{90}/R_{50}$) as a function of the isophotal limit. The solid and dotted lines denote the BCG and control samples respectively. Error bars are the 68.3% confidence levels of the median value.

H_0 , and taking $V - r = 0.3 \pm 0.1$, Krick et al. 2006) tend to have ‘cored’ luminosity profile, while galaxies fainter than $M_V = -20.5$ mag (corresponding to $M_r \approx -21.1$ mag) tend to have ‘power-law’ luminosity profiles (see also Rest et al. 2001; Lauer et al. 2005). Other works (e.g., Rest et al. 2001) show that bright galaxies are slowly rotating, boxy systems (Davies et al. 1983) while faint elliptical galaxies are fast rotating, disk systems (Bender 1988; Bender et al. 1989; Nieto et al. 1988). However, BCGs appear to somewhat contradict with this trend: some very luminous BCGs still have disk isophotes. The flattening in elliptical galaxies can arise either from an-isotropic motions or from rotation. Faint ellipticals appear to be flattened by rotation (e.g., van den Bosch et al. 1994; Lauer et al. 2005), while the luminous ones may be supported by an-isotropic motions. As we have shown in the last subsection, BCGs may have experienced fairly recent merging events, and thus may still retain some of the orbital angular momentum from merging, and their isophotes may be disk.

4.4 Scaling relations

There have already been many works on the scaling relation of BCGs based on homogeneous BCG samples (Bernardi et al. 2007; Desroches et al. 2007; von der Linden et al. 2007; Lauer et al. 2007). However, so far no work has investigated how the slopes change with the isophotal limit, which can in principle provide more knowledge of the dynamical structure of BCGs.

4.4.1 The size-luminosity relation

The left panels of Fig. 11 show how the size (R_{50}) and luminosity (L_r) vary with the isophotal limits. It is clear that the size (R_{50}) and luminosity of BCGs increase more sharply

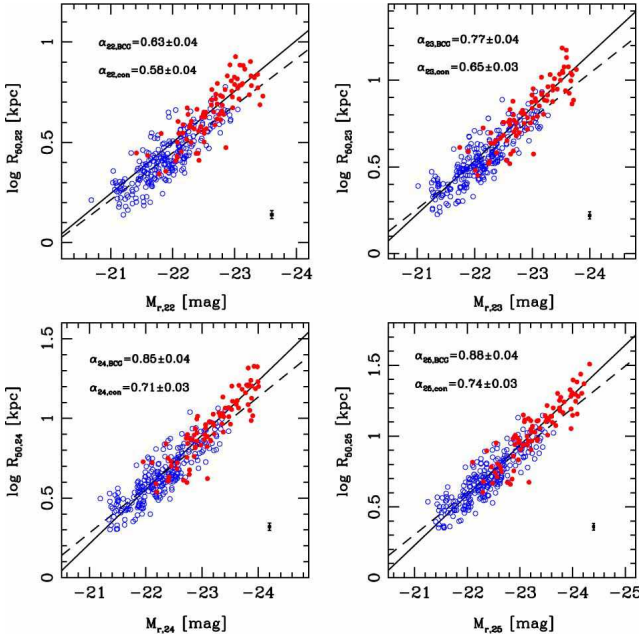


Figure 12. The size-luminosity relation for BCGs (red solid circles) and the control sample (blue open circles) for four isophotal limits, 22, 23, 24, and 25 mag arcsec⁻² respectively. The median error bar for the data points is indicated in the bottom right corner of each panel. The black solid and dashed lines are the best power-law fits for the BCGs and control sample respectively. The power-law index α ($R_{50} \propto L^\alpha$) is shown at the top of each panel.

than that of the control sample as the isophotal limit becomes deeper. The right panel shows how the mean surface brightness within R_{50} ($\langle \mu_{50} \rangle$) and the concentration factor ($C' = R_{90}/R_{50}$) vary with the isophotal limit. We can see that $\langle \mu_{50} \rangle$ of BCGs decreases more sharply than that of control sample, but $C' = R_{90}/R_{50}$ of BCGs has the same trend as that of the control sample as the isophotal limit becomes deeper. Therefore, BCGs appear to have significantly larger average sizes and are more diffuse in surface brightness. These trends agree with those found in previous studies (e.g., Lugger 1984; von der Linden et al. 2007).

Fig. 12 shows the size-luminosity relations for our BCGs and the control sample, measured to four isophotal limits, 22, 23, 24 and 25 mag/arcsec² respectively. The solid and dotted lines in each panel show the best power-law ($R_{50} \propto L^\alpha$) fits; the α value is indicated at the top left corner of each panel.³

Clearly the size-luminosity relation becomes steeper as the isophotal limit becomes fainter for both the BCG and the control sample. However, we can also see that the size-luminosity relation for BCGs is steeper than that of the control sample at the same isophotal limit. In particular, the

size-luminosity relations for BCGs is already slightly steeper (but not very statistically significant) than those of the bulk of ellipticals when the isophotal limit is 22 mag arcsec⁻², corresponding to a physical half-light radius of about 5 kpc (see Fig. 11). It indicates that the deviation of size-luminosity relation for BCGs from that of bulk of ellipticals may already occur for the inner regions of ellipticals, and thus is not because most BCGs have extended stellar halos. Rather, this suggests the deviations arise from different dynamical structures of BCGs from the bulk of ellipticals. Bernardi et al. (2007) arrived at a similar conclusion by comparing the size-luminosity relations for BCGs with and without extended stellar envelopes (see also von der Linden 2007).

The power-law index (0.88 ± 0.04) for the size-luminosity relation we derived for BCGs at an isophotal limits of 25 mag/arcsec² is slightly smaller than the value (0.92) obtained by Bernardi et al. (2007), but the power-law index (0.74 ± 0.03) for the control sample at the same isophotal limit is a bit larger than their value (0.62). The difference in the slope measured by us and by Bernardi et al. (2007) may be because we measure the isophotal magnitudes by integrating the observed surface brightness profiles directly, while Bernardi et al. (2007) measured the magnitude using a de Vaucouleurs or Sérsic model for the surface brightness profile. In fact, when we use the same method as Bernardi et al. (2007) to perform photometry, the power-law index for the size-luminosity relation we obtain is almost the same (0.93 ± 0.03) as that of Bernardi et al. (2007), indicating that different ways of photometry can give different power-law indices in the size-luminosity relation.

von der Linden (2007) also derived the size-luminosity relation down to 23 mag arcsec⁻² for their BCGs. The slope they derived is $\alpha = 0.65 \pm 0.02$, similar to that for their control sample ($\alpha = 0.63 \pm 0.02$). Our slope for the BCGs (0.77 ± 0.04) is steeper than their value at the same isophotal limit, while the slope for our control sample ($\alpha = 0.65 \pm 0.03$) agrees well with theirs. We have 66 overlapping galaxies with the BCG samples used by von der Linden et al. (2007). If we use only these galaxies, we derive a slope similar to theirs. Our steeper slope appears to arise from the fact that our BCGs are brighter since their sample includes more fainter BCGs which makes their slope shallower (von der Linden 2007, private communication). Therefore, the sample construction also influences the power-law index in the size-luminosity relation.

The power-law index $\alpha = 1.18 \pm 0.06$ in the size-luminosity relation by Lauer et al. (2007) for their core galaxies with $M_V \leq -21$ (most core galaxies with $M_V \leq -22$ are BCGs) measured in a similar way as Bernardi et al. (2007) is significantly steeper than those of Bernardi et al. (2007), von der Linden (2007) and our results. It again illustrates that how samples are constructed and the methods used to do the photometry lead to different power-law indices in the size-luminosity relation. Comparisons between different studies should be aware of this.

4.4.2 The Faber-Jackson relation and Fundamental plane

It is well known that the luminosities and velocity dispersions of many early type galaxies satisfy the Faber-Jackson relation, $L \propto \sigma^\beta$, where $\beta \approx 4$ (Faber & Jackson 1976). Given that the SDSS spectra were taken within a 3'' fiber

³ Notice that the intrinsic scatters in the data points are much larger than the statistical error bars, and so the formal χ^2 per degree of freedom is large, indicating the presence of systematics. To approximately account for these, we renormalised the statistical errors by a constant factor until the χ^2 per degree of freedom is unity. The errors on the power-law indices are obtained using these renormalised errors. A similar procedure was adopted in von der Linden et al. (2007).

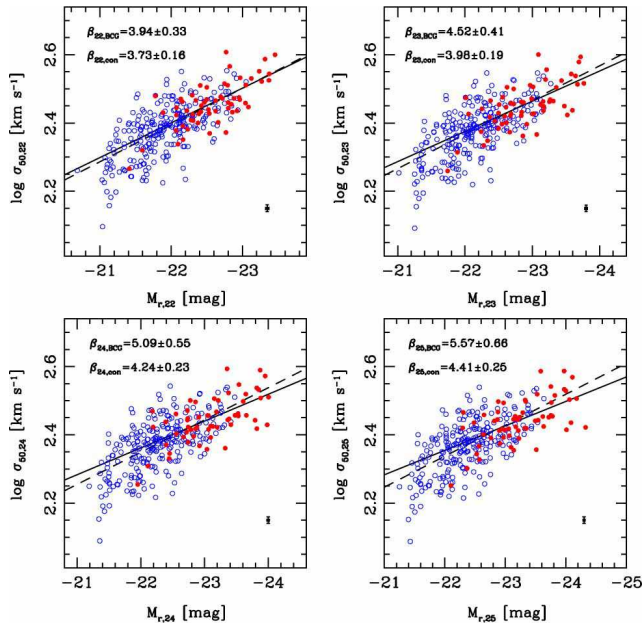


Figure 13. The Faber-Jackson relation for the 59/85 BCGs and 244 control sample galaxies with spectroscopic information for four different isophotal limits (22, 23, 24, and 25 mag arcsec⁻²) respectively. The symbols are the same as in Fig. 12. The power-law indices β are shown at the top of each panel for the BCGs and the control sample. The median error bar in the velocity dispersion is shown at the bottom right in each panel.

aperture (Jørgensen et al. 1995; Bernardi et al. 2003a), we correct the velocity dispersions for BCGs and the control sample following von der Linden et al. (2007, see their equation 4). The uncorrected value of σ for each BCG is shown in Column 5 of Table 2.

Fig. 13 shows the $L - \sigma$ relation for 59 out of 85 BCGs and the control sample with SDSS spectral information, measured to four different isophotal limits, 22, 23, 24, and 25 mag arcsec⁻². Clearly at a given surface brightness limit, the slope for BCGs in the Faber-Jackson relation is steeper than that of the bulk of early type galaxies. The index β for both the BCG and control samples increases as the isophotal limits become deeper. The β value for the control sample is around 4, consistent with the canonical value for the Faber-Jackson relation. However, this is not the case for BCGs: only when the isophotal limit is 22 mag arcsec⁻², corresponding to the inner region of BCGs, β is about 4. For deeper isophotal limits, the β values for BCGs are significantly larger, approaching 5.6 for a surface brightness limit of 25 mag arcsec⁻². von der Linden (2007) found $\beta = 5.32 \pm 0.37$ for their BCGs at an isophotal limit of 23 mag arcsec⁻², which is within 2σ of our value ($\beta = 4.52 \pm 0.41$). For their control samples, they found $\beta = 3.93 \pm 0.21$, within 1σ of our result ($\beta = 3.98 \pm 0.19$). Lauer found $\beta = 6.5 \pm 1.3$ for their core galaxies with $M_V < -21$, which is significantly larger than those of values mentioned above. Note that the sample Lauer et al. (2007) used is not a pure BCG sample, although most of their core galaxies with $M_V < -22$ are BCGs.

The steeper power-law indices in the size-luminosity and (to a less extent) in the Faber-Jackson relations may arise because BCGs are brighter than the control sample

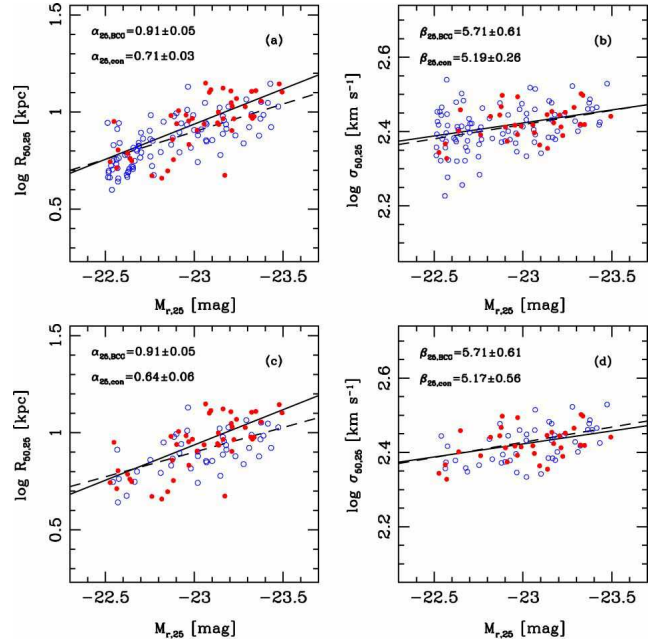


Figure 14. The size-luminosity relation (left) and Faber-Jackson relation (right) for the BCG and control sample galaxies at $-23.5 \leq M_{r,25} \leq -22.5$. The top panels use all 94 control galaxies and 45 BCGs in this luminosity range. The bottom panels are the results for one realisation for 45 BCGs and randomly selected 45 control galaxies with the same luminosity distribution. The symbols are the same as in Fig. 12. The power-law indices are shown at the top of each panel for each sample.

or because there are intrinsic differences between BCGs and the bulk of elliptical galaxies. In order to differentiate these two possibilities, we repeat the above analysis for our BCG and control samples in the same magnitude range, $-23.5 \leq M_{r,25} \leq -22.5$ (see §2). Fig. 14 shows the size-luminosity (left) and Faber-Jackson (right) relations. The top panels use all the 94 control-sample galaxies and 45 BCGs within the luminosity range. Since Fig. 1 shows the control sample is still fainter on average than the BCG sample within this narrow range, we have randomly selected 45 out of the 94 control-sample galaxies so they match well with the luminosity distribution of the 45 BCGs. The statistical results for different realisations are similar; the bottom panels shows the results for one realisation. From this figure, we clearly see that the power-law indices for the size-luminosity relations for BCGs are steeper than those for bright non-BCG elliptical galaxies; the power-law indices for the Faber-Jackson relations are also steeper, but only at $\sim 1\sigma$ levels, and so are not statistically significant. To summarise, the data are consistent with a scenario where the cluster environment plays an important role on the BCG formation. However, the numbers of galaxies in our control and BCG samples are still too small to differentiate the two possibilities mentioned above.

Fig. 15 shows the fundamental plane for our BCGs and the control sample. While they appear to have different power-law slopes in the Faber-Jackson relation, both BCGs and the control sample follow roughly the same fundamental plane, although the scatters in the BCGs appear smaller. At bright isophotal limits, $\mu = 22$, and 23 mag arcsec⁻², the

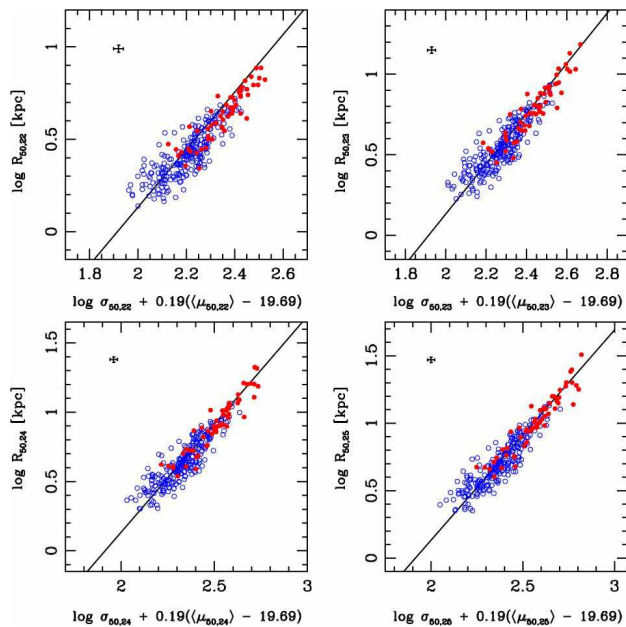


Figure 15. Fundamental planes for the 59 BCGs with spectra (dots) and 244 control sample (open circles) for four different isophotal limits respectively. The solid line in each panel is the fundamental plane determined by Bernardi et al. (2003b) using a uniform sample of ~ 9000 early type galaxies. The median error bars are shown at the top left.

fundamental planes for BCGs and the control samples appear to differ somewhat. These results are in good agreement with Bernardi et al. (2007).

5 SUMMARY

In this paper we have studied the properties of 85 BCGs carefully selected from the C4 cluster catalog (Miller et al. 2005). To address the problems of the SDSS pipeline PHOTO in crowded fields and for large galaxies, we have performed our own photometry for these BCGs, as well as for a control sample of galaxies in similar redshift and apparent magnitude ranges. Particular attention was paid to accurate extraction of the sky background in clusters using a method developed for high-precision photometry for large, nearby spiral galaxies (Zheng et al. 1999; Wu et al. 2002, see §3). It came as somewhat a surprise to us that the simple recipe of von der Linden et al. (2007) gives surface brightness profiles similar to ours, and hence for many statistical purposes their simple recipe can be adopted as a more efficient alternative.

We analysed the surface brightness properties of our BCGs using the $\eta(r)$ profiles (see eq. 1). We demonstrate that its gradient, $\gamma(r) \equiv d\eta(r)/d\log(r)$, can be used as an indicator of extended envelopes of cD galaxies (Patel et al. 2006). Furthermore, we find that the depth of valley, D_{\min} in the $\gamma(r)$ profiles can be used to quantitatively measure the properties of the plateaus in the surface brightness profiles. Generally, the deeper the valleys are (corresponding to a larger value of D_{\min}), the flatter and wider the plateaus are in the $\eta(r)$ profiles. However, the D_{\min} parameter appears to vary in a continuous way with the galaxy parameters, such as their size and luminosity. While there is a

clear trend that more luminous and larger BCGs have larger stellar halos, the continuous variation makes it difficult to un-ambiguously classify cD or non-cD galaxies based on the surface brightness profiles alone.

We measured the photometric properties of galaxies to four different isophotal limits, 22, 23, 24, and 25 mag arcsec $^{-2}$, and used these to investigate the scaling laws and their dependence on these limits. The latter is of particular relevance as some previous investigations derived scaling relations for BCGs using different samples and different isophotal limits (e.g., the study of von der Linden et al. 2007 used an isophotal limit of 23 mag arcsec $^{-2}$). We find that the size-luminosity relation and Faber-Jackson ($L - \sigma$) relations of BCGs are consistent with being steeper than those of the bulk of early type galaxies for a control sample selected within the same absolute magnitude range ($-23.5 < M_{r,25} < -22.5$), although the latter is not statistically significant due to the limited sample sizes.

Furthermore, as the photometric limit becomes deeper, the size-luminosity relation for BCGs and the bulk of the ellipticals becomes steeper. However, there are already (small) differences between BCGs and regular ellipticals at 22 mag arcsec $^{-2}$, a surface brightness that probes the inner parts of galaxies. This, together with the relatively small difference in the scaling relations between 24 mag arcsec $^{-2}$ and 25 mag arcsec $^{-2}$, suggests that there may be intrinsic differences in the dynamic structures between BCGs and the bulk of early type galaxies (Bernardi et al. 2007; Lauer et al. 2007). One possibility may be that the amount of dark matter in the central parts of BCGs and regular ellipticals is different (von der Linden et al. 2007), or perhaps the relative importance of anisotropy and rotation may be different. In this context, it is interesting to note that we find a large fraction of very luminous early type galaxies with disk isophotes. This appears to somewhat contradict with the usual expectation that the most luminous galaxies should show boxy isophotes. Also notice that it is difficult to measure high-redshift galaxies to very faint surface brightness due to the cosmological dimming. Thus a proper comparison between local and high-redshift samples will need to explicitly account for the surface brightness dependence we found in the paper.

In this work we uncovered four strong dry merger candidate BCGs (see Fig. 8), three of which have two close nuclei within 10 kpc and with nearly identical radial velocities. We also found another 10 BCGs in our sample with possible dry merger signatures (see Fig. 9), as advocated by Bell et al. (2006). This strongly suggests merging at the centre of clusters is an important physical process that affects a variety of properties of BCGs, both in photometry and kinematics. An analysis of the statistics for the fraction of dry mergers in BCGs is ongoing and the results will be reported elsewhere.

ACKNOWLEDGEMENTS

We thank C. N. Hao, Simon White for discussions, and in particular A. von der Linden for sharing data, helpful discussions and comments on a draft. We acknowledge Dr. Tod Lauer, the referee, for a constructive report that improved the paper. This project is supported by the NSF of China 10333060, 10273012, 10640430201, 10773014 and 973 pro-

grams No. 2007CB815405 and 2007CB815406. SM acknowledges the Chinese Academy of Sciences and the Alexander von Humboldt Foundation. Funding for the creation and distribution of the SDSS Archive has been provided by the Alfred P. Sloan Foundation, the Participating Institutions, the National Aeronautics and Space Administration, the National Science Foundation, the U.S. Department of Energy, the Japanese Monbukagakusho, and the Max Planck Society. The SDSS Web site is <http://www.sdss.org/>. The SDSS is managed by the Astrophysical Research Consortium (ARC) for the Participating Institutions. The Participating Institutions are The University of Chicago, Fermilab, the Institute for Advanced Study, the Japan Participation Group, The Johns Hopkins University, the Korean Scientist Group, Los Alamos National Laboratory, the Max-Planck-Institute for Astronomy (MPIA), the Max-Planck-Institute for Astrophysics (MPA), New Mexico State University, University of Pittsburgh, Princeton University, the United States Naval Observatory, and the University of Washington.

REFERENCES

- Bell E. F. et al., 2006, *ApJ*, 640, 241
 Bender R., 1988, *A&A*, 193, L7
 Bender R., Döbereiner S., Möllenhoff C., 1988, *A&AS*, 74, 385
 Bender R., Surma P., Doebereiner S., Moellenhoff C., Madejsky R., 1989, *A&A*, 217, 35
 Bernardi M. et al., 2003a, *AJ*, 125, 1817
 Bernardi M. et al., 2003b, *AJ*, 125, 1866
 Bernardi M., Hyde J. B., Sheth R. K., Miller C. J. Nichol R. C., 2007, *AJ*, 133, 1741
 Bertin E., Arnouts S., 1996, *A&AS*, 117, 393
 Binney J., Merrifield M., 1998, *Galactic Astronomy* (Princeton: Princeton Univ. Press)
 Blanton M. R. et al., 2003a, *ApJ*, 592, 819
 Blanton M. R. et al., 2003b, *ApJ*, 594, 186
 Blanton M. R. et al., 2005, *AJ*, 129, 2562
 Blanton M. R., Roweis S., 2007, *AJ*, 133, 734
 Brough S., Collins C. A., Burke D. J., Lynam P. D., Mann R. G., 2005, *MNRAS*, 364, 1354
 Cowie L. L., Binney J., 1977, *ApJ*, 215, 723
 Davies R. L., Efstathiou G., Fall S. M., Illingworth G., Schechter P. L., 1983, *ApJ*, 266, 41
 De Lucia G., Blaizot J., 2007, *MNRAS*, 375, 2
 Desroches Louis-Benoit, Quataert E., Ma Chung-Pei, West A. A., 2007, *MNRAS*, 377, 402
 de Vaucouleurs G., 1948, *Ann. Astrophys.*, 11, 247
 Faber S. M. et al., 1997, *AJ*, 114, 1771
 Faber S. M., Jackson R. E., 1976, *ApJ*, 204, 668
 Fabian A. C., 1994, *ARA&A*, 32, 277
 Fabian A. C., Nulsen P. E. J., 1977, *MNRAS*, 180, 479
 Fan X. et al., 1996, *AJ*, 112, 628
 Gallagher J. S., Ostriker J. P., 1972, *AJ*, 77, 288
 Gao L., Loeb A., Peebles P. J. E., White S. D. M., Jenkins A., 2004, *ApJ*, 614, 17
 Gonzalez A. H., Zabludoff A. I., Zaritsky D., 2005, *ApJ*, 618, 195
 Graham A., Lauer T. R., Colless M., Postman M., 1996, *ApJ*, 465, 534
 Hao C. N., Mao S., Deng Z. G., Xia X. Y., Wu H., 2006, *MNRAS*, 370, 1339; erratum, *MNRAS*, 373, 1264
 Jones C., Forman W., 1984, *ApJ*, 276, 38
 Jørgensen I., Franx M., Kjaergaard P., 1995, *MNRAS*, 276, 1341
 Kjaergaard P., Jørgensen I., Moles M., 1993, *ApJ*, 418, 617
 Koester B. P. et al., 2007, *ApJ*, 660, 239
 Krick J. E., Bernstein R. A., Pimbblet K. A., 2006, *AJ*, 131, 168
 Laine S., van der Marel R. P., Lauer T. R., Postman M., O'Dea C. P., Owen F. N., 2003, *AJ*, 125, 478
 Lauer T. R., 1985, *MNRAS*, 216, 429
 Lauer T. R., 1988, *ApJ*, 325, 49
 Lauer T. R. et al., 2005, *AJ*, 129, 2138
 Lauer T. R. et al., 2007, *ApJ*, 662, 808
 Lin Y.-T., Mohr J. J., 2004, *ApJ*, 617, 879
 Lugger P. M., 1984, *ApJ*, 286, 106
 Matthews T. A., Morgan W. W., Schmidt M., 1964, *ApJ*, 140, 35
 Merritt D., 1985, *ApJ*, 289, 18
 Michard R., 2002, *A&A*, 384, 763
 Miller C. J. et al., 2005, *AJ*, 130, 968
 Nieto J.-L., Capaccioli M., Held V. E., 1988, *A&A*, 195, L1
 Oegerle W. R., Hoessel J. G., 1991, *ApJ*, 375, 15
 Oemler A., Jr., 1973, *ApJ*, 180, 11
 Oemler A., Jr., 1976, *ApJ*, 209, 693
 Ostriker J. P., Hausman M. A., 1977, *ApJ*, 217, L125
 Ostriker J. P., Tremaine S. D., 1975, *ApJ*, 202, L113
 Patel P., Maddox S., Pearce F. R., Aragón-Salamanca A., Conway E., 2006, *MNRAS*, 370, 851
 Petrosian V., 1976, *ApJ*, 209, L1
 Postman M., Lauer T. R., 1995, *ApJ*, 440, 28
 Rest A., van den Bosch F. C., Jaffe W., Tran H., Tsvetanov Z., Ford H. C., Davies J., Schafer J., 2001, *AJ*, 121, 2431
 Richstone D., 1975, *ApJ*, 200, 535
 Richstone D., 1976, *ApJ*, 204, 642
 Schombert J. M., 1986, *ApJS*, 60, 603
 Schombert J. M., 1987, *ApJS*, 64, 643
 Schombert J. M., 1988, *ApJ*, 328, 475
 Sérsic J. L., 1968, *Atlas de Galaxies Australes* (Cordoba: Observatorios Astronomica)
 Shen S. et al., 2003, *MNRAS*, 343, 978
 Shimasaku K. et al., 2001, *AJ*, 122, 1238
 Smith G. P., Kneib J.-P., Smail I., Mazzotta P., Ebeling H., Czoske O., 2005, *MNRAS*, 359, 417
 Stoughton C. et al., 2002, *AJ*, 123, 485
 Strateva I. et al., 2001, *AJ*, 122, 1861
 Tran K.-V., van Dokkum P. G., Franx M., Illingworth G. D., Kelson D. D., Schreiber N. M. F., 2005, *ApJ*, 627, L25
 van den Bosch F. C., Ferrarese L., Jaffe W., Ford H. C., O'Connell R. W., 1994, *AJ*, 108, 1579
 van Dokkum P. G., 2005, *AJ*, 130, 2647
 von der Linden A. et al., 2007, *MNRAS*, 379, 867
 White S. D. M., 1976, *MNRAS*, 174, 19
 White S. D. M. et al., 2005, *AAP*, 444, 365
 Wu H. et al., 2002, *AJ*, 123, 1364
 Wu H., Shao Z. Y., Mo H. J., Xia X. Y., Deng Z. G., 2005, *ApJ*, 622, 244
 Zibetti S., White S. D. M., Schneider D. P., Brinkmann J., 2005, *MNRAS*, 358, 949
 Zheng Z. Y. et al., 1999, *AJ*, 117, 2757